Successive Steps of 2D and 3D Transition in the Flow Past a Rotating Cylinder at Moderate Reynolds Numbers

R. ELAKOURY[1], G. MARTINAT[1], M. BRAZA[1], R. PERRIN[1], Y. HOARAU[2], G. HARRAN[1], D. RUIZ[3]

[1] *Institut de Mécanique des Fluides de Toulouse, CNRS/INPT UMR N° 5502*
Av. du Prof. Camille Soula, 31400 Toulouse, France

[2] *Institut de Mécanique des Fluides et des Solides de Strasbourg,CNRS/ULP UMR N° 7507*
2 rue Boussingault, 67000 Strasbourg, France

[3] *ENSEEIHT, CNRS/IRIT UMR N° 5505, Toulouse, France*

Abstract. The flow past a rotating circular cylinder, placed in a uniform stream, is investigated by means of 2D and 3D direct numerical simulations, using the finite-volume version of the code ICARE/IMFT. The flow transition is studied for Reynolds numbers from 40 to 500, and for rotation rates α (ratio of the angular and the free-stream velocities) up to 6. For a fixed Reynolds number, different flow patterns are observed as α increases: Von-Kármán vortex shedding for low rotation rates, suppression of the vortex shedding at higher α, appearing of a second mode of instability for a high interval of α where only counter clockwise vortices are shedd, and steady state flow for very high rotation speeds where the rotation effects keep the vortex structure near the wall and inhibit detachment. Three dimensional computations are carried out showing that the secondary instability is attenuated under the rotation effect. The linear and non-linear growth of the 3D flow transition are quantified using the Ginzburg-Landau global oscillator model. The analysis of the coherent structures under the rotation effect is performed by the proper orthogonal decomposition, as well the pattern reconstruction using the first POD modes.

Key words: rotation, transition, DNS, POD.

1. Introduction

The vortex dynamics of the flow around a fixed circular cylinder have been the objective of a considerable number of investigations. Comparatively, less work has been performed in the case of a rotating cylinder. This paper aims to study the transition in the wake past a circular cylinder under the rotation effect (fig. 1.). The flow depends mainly on two parameters: The Reynolds number $Re = \frac{U_\infty D}{\nu}$ and the rotation rate $\alpha = \frac{D\omega}{2U_\infty}$, where U_∞ is the free-stream velocity, D the cylinder diameter, ν the kinematic viscosity and ω the angular velocity of the cylinder.

Earliest experiments on the flow past a circular rotating cylinder where performed by Reid [18], Prandtl [17] and Thom [21, 22]. More recently, the early phase of the establishment of the flow around a cylinder started impulsiveley into rotation and translation was investigated experimentally by Coutanceau and Ménard [9], and numerically by Badr and Dennis [3], for moderate Reynolds numbers ($Re \leq 1000$). The same study was performed both theoratically and experimentally by Badr et

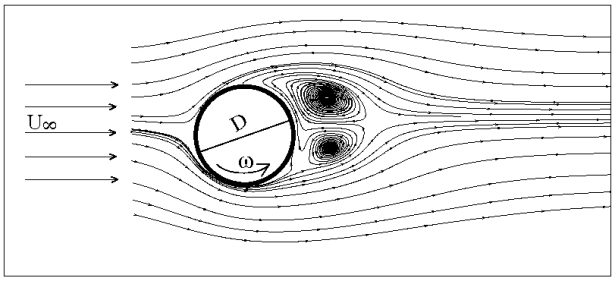

Figure 1. shematic of the physical problem

al. [2], in higher Reynolds number range $10^3 \leq Re \leq 10^4$. The same initial stage of the vortex shedding was studied numerically by Chang and Chern [7], for $10^3 \leq Re \leq 10^6$ end $0 \leq \alpha \leq 2$, and later by Nair et al. [14] who provided detailed results for $Re = 3800$ and $\alpha = 2$.

Concerning the estabilished state, a number of investigation were performed at low and moderate Reynolds numbers, showing the suppression of the Von-Kármán vortex shedding when the rotation rate increases. Stojković et al.[19] were the first to notice the existence of a second shedding mode for $4.8 \leq \alpha \leq 5.15$ at $Re = 100$. The two-dimensional numerical study of Stojković et al. [20] confirmed the existence of this second mode in the Reynolds number range $60 \leq Re \leq 200$. Different flow regimes as rotation speed increases were also investigated numerically by Mittal and Kumar [13], at $Re = 200$, $0 \leq \alpha \leq 5$. Later, Cliffe and Tavener [8] studied the effect of the rotation of a cylinder on the critical Reynolds and Strouhal numbers at the hopf bifurcation point. They noticed the restabilization of steady flows at large blockage ratios as the Reynolds number is increased even for non-rotating cylinders.

The different flow regimes are studied in this paper for the flow around a rotating circular cylinder by means of 2D and 3D computations. The outlines of the finite-volume formulation of the ICARE code of the IMFT, Braza et al. [6], Persillon and Braza [16] are presented in §2. Detailed two-dimensional analysis for the flow transition is performed in §3. for Reynolds numbers from 40 to 500, and for rotation rates up to 6. §4. analyses the onset of the three-dimensional transition under the rotation effect. The ampilification of the secondary instability is studied by means of the global oscillator model. The study of the coherent structures motion is next carried out by means of the proper orthogonal decomposition as well the pattern reconstruction in §5.

2. Principles of numerical method

The 2D and 3D simulations were carried out using the code ICARE of the IMFT, in its finite-volume version. The governing equations are the continuity and the Navier-Stokes equations for an incompressible fluid, written in general curviliner coordinates in the (x, y) plane, while the $z-$ component (in the spanwise direction) is in cartesian coordinates. The numerical method is based on a pressure-velocity formulation using a predictor-corrector pressure sheme of the same kind as the one reported by Amsden and Harlow [1], extended in the case of an implicit formulation by Braza et al. [6]. The temporal discretistation is done adopting the Peaceman

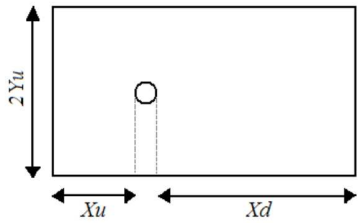

Figure 2. Computational domain

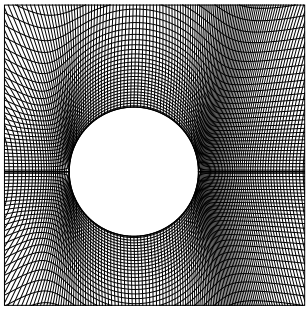

Figure 3. magnification of the grid around the cylinder

	Nx	Ny	N_w	Xu	Xd	Yu
$Re \leq 200$	250	100	43	8.95	20.51	7.42
$Re = 200$; $4.35 < \alpha < 4.85$	352	112	43	9.40	42.37	8.50
$Re = 300$	303	120	47	11.50	23.70	10.02
$Re = 500$	360	146	61	11.54	23.41	10.21

Table 1. Characteristics of the different computational domains; Nx and Ny: number of points in the x- and y-direction respectively; $2N_w$: number of points on the cylinder surface; Xu and Xd: upstream and downstream length; $2Yu$: vertical width of the domain; see also figure 2

and Rachford [15] scheme in an Alternating Direction Implicit formulation. The method is second-order accurate in time and space. The staggered grids by Harlow and Welch [10] are employed for the velocity and pressure variables.

H-type grids are used because this kind of grid offers the possibility to introduce more physical boundary conditions on the external boundaries and it avoids branch-cut lines. A zoom of the grid around the obstacle is shown in figure 3. The characteristics of the different grids used are shown on table 1. The grid used for the 3D simulation is $(250 \times 100 \times 80)$ where the same grid is repeated in all dz sections. The spanwise length of the computational domain is $12D$ where D represents the cylinder diameter, A careful study of the numerical parameters and of the dimensions of the computational domain had been conducted for the final choice, in respect of the grid and the spanwise distance independence of the results, as well as for the 2D study.

The boundary conditions are those specified in Persillon and Braza [16]. Concerning the spanwise free edges of the computational domain, periodic boundary conditions are applied.

3. Successive stages in the two-dimensional transition

The flow transition is analysed for Reynolds numbers 40 to 500 for different rotation rate numbers, α varying from 0 to 6. The changes in the flow pattern are studied by means of the averaged and instantaneous streamlines, of the global parameters and of the vorticity fields.

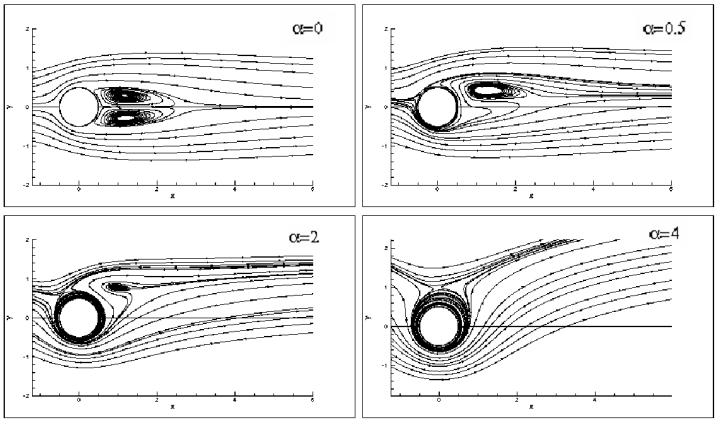

Figure 4. streamlines for different rotation rate values, $Re = 40$

3.1. Steady state flow at $Re = 40$

For $Re < 48$, the flow remains steady for all the rotation rates investigated. In the fixed cylinder case, the flow shows two symmetric vortices attached to the cylinder. The rotation causes a loss of symmetry as shown in figure 4; stagnation points are attained in the upper part of the cylinder. As a consequence of the Magnus effect, the lift coefficient increases and the drag coefficient decreases.

Detailed flow computations were carried out for higher Reynolds numbers up to 500; similar flow regimes appear as α increases. In the following section, The $Re = 300$ case is detailed.

3.2. Successive stages of 2D transition in the flow around a rotating cylinder at $Re = 300$

Different flow patterns

For low rotation rates, $\alpha < 2.5$, the flow is unsteady, qualitatively similar to the fixed cylinder case, where the Von Kármán vortex shedding is observed, asymmetric towards the upper side of the cylinder due to the rotation sense. For higher rotation rates, the vortex shedding is suppressed; the flow remains steady until a rotation rate of 3.9 where a second mode of instability (mode II) appears for $3.9 < \alpha < 4.8$. In this interval, only counter-clockwise vortices are shedd from the upper side of the cylinder in a periodic motion. This second mode of instability is due to the increasing of the rotation rate and of the velocity gradient between the two sides of the cylinder, in association with the strong viscous effect near the wall. Thus the steamlines that are closed around the cylinder start to have an oval-like form. The fluid flow forces this structure to be more elongated until detachement. Mode II disappears for higher rotation rates where the rotation effects keep the vortex structure near the wall and inhibit detachement. Figure 5 shows the different flow configurations for $Re = 300$ as α increases.

Global parameters

Figure 6 shows the evolution of the Strouhal number $St = \frac{fD}{U_\infty}$ as a function of α. For low rotation rates in mode I, St is practically constant, and it shows a reduction as

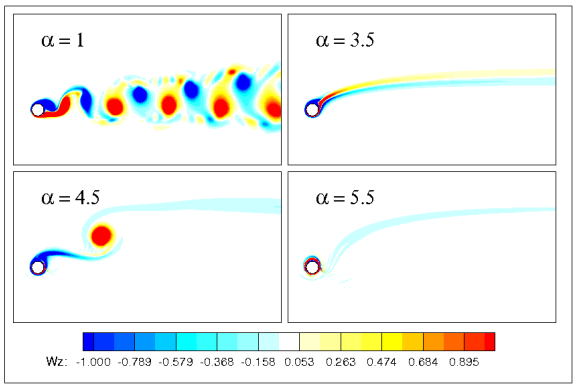

Figure 5. Iso-vorticity contours for different states at $Re = 300$

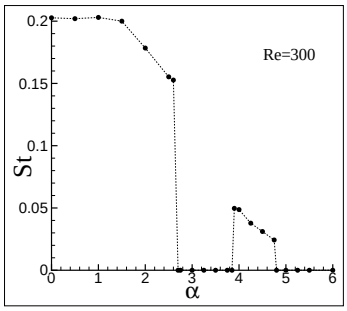

Figure 6. Stouhal number St versus rotation rate α at $Re = 300$

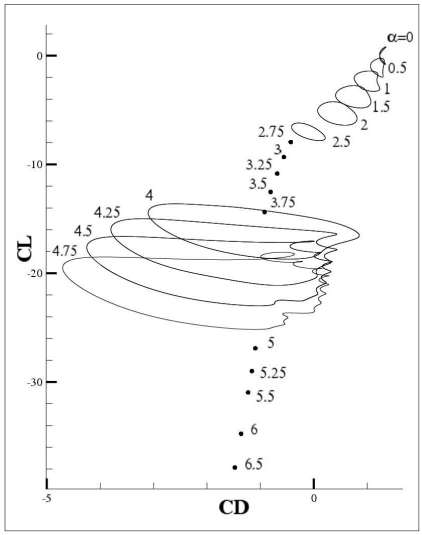

Figure 7. phase diagram (C_D, C_L) for different values of α at $Re = 300$

a function of α before the first bifurcation. St in mode II also decreases in the range of $3.9 \leq \alpha \leq 4.8$. Therefore, the effects of increasing rotation have the tendency to diminish the instability mode and even to make it vanish.

Concerning the lift and the drag coefficients, figure 7 represents the phase diagram (C_D, C_L). For $\alpha = 0$, the phase plot is like a figure of 8, because in each cycle, two vortices of equal strenght are released from the upper and the lower side of the cylinder, and the frequency of the drag variation is twice that of the variation of lift. The rotation introduces asymmetry in the strenght and the location of the positive and negative vortices. The phase plots form closed lobes in both mode I and mode II, corresponding to a periodic flow. The size of each lobe shows the amplitude of fluctuation of the global coefficients. It is shown that the amplitude of the drag coefficient increases as α increases. In the mode II, large amplitudes for C_D and C_L are shown; in this case, the periodic flow is more complex than the mode I case.

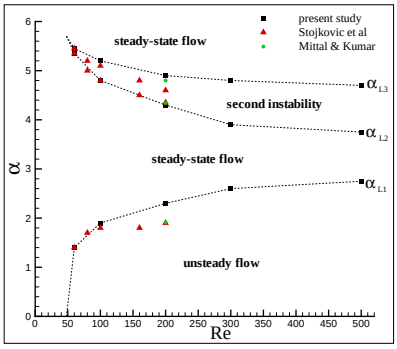

Figure 8. stability diagram for different Reynolds numbers and rotation rates

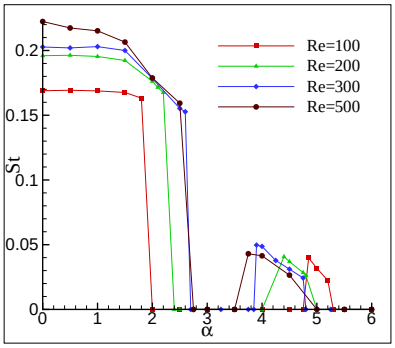

Figure 9. St as a function of α for different Re

3.3. Influence of the Reynolds number

Similar flow regimes appear as a function of the Reynolds number. The Von-Kármán vortex shedding is observed for low rotation rates $\alpha < \alpha_{L1}$, α_{L1} increasing as Re increases. The flow is steady for $\alpha_{L1} < \alpha < \alpha_{L2}$. Mode II of instability appears in the range $\alpha_{L2} < \alpha < \alpha_{L3}$. α_{L2} and α_{L3} decrease as the Reynolds number increases where viscous effects are reduded, and the flow approaches the potentiel theory flow for lower rotation rates. The critical α values are presented in figure 8 for different Reynolds numbers in comparison with previous results of Mittal and Kumar [13] and Stojković et al. ([20],[19]). This figure shows also that the critical Reynolds number of appearance of the first flow unsteadiness increases with respect to α. Figure 9 shows the evolution of the Strouhal number for $Re = 100$, 200, 300 and 500

4. Three-dimensional transition

This section analyses the onset of the 3D transition phenomena under the rotation effect concerning the coherent structures in the wake. Without rotation, at Reynolds number 200 the three-dimensionality starts from an amplification of the w component versus time in the near wake. This displays a linear amplification rate following a non-linear state that leads finally to a saturation state as reported by Persillon and Braza [16]. The w amplification announces the development of a secondary instability concerning the 3D modification of the von Kármán mode that starts to display a regular spanwise undulation (mode A). The spanwise undulation is shown in figure 10. The same kind of flow where wall rotation is applied ($\alpha = 1.5$) displays however a total damping of the amplification mode(figure 11). Therefore the rotation attenuates the secondary instability and increases the critical Reynolds number of appearance of this instability. Indeed, at higher Reynolds number, $Re = 300$, the 3D undultaion is clearly shown for α=0.5 (figure 14).

The amplification of the above instability can be studied by means of the Landau global oscillator model, Mathis et al.[12].

$$\frac{\partial A}{\partial t} = \underbrace{\sigma_r A}_{linear\ growth} - \underbrace{l_r |A^3|}_{non\ linear} + \underbrace{\mu_r \frac{\partial^2 A}{\partial z^2}}_{3D-undulation} \tag{1}$$

The real part of the coefficients σ_r and l_r can be evaluated by the present DNS study,

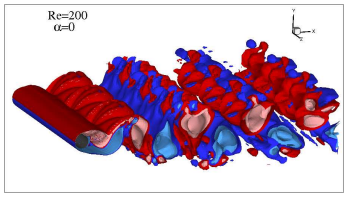

Figure 10. Iso-vorticity surfaces of the 3D fields, $Re = 200$, $\alpha = 0$

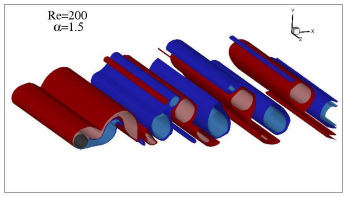

Figure 11. vanishing of the 3D undulation with the rotation,$Re = 200$, $\alpha = 1.5$

that provides the amplitude variation as a function of period. σ_r can be evaluated by the $log(A)$ variation as a function of time. For $Re = 200$, $\alpha = 0$, $\sigma_r = 0.013$ and for $Re = 300$, $\alpha = 0.5$, $\sigma_r = 0.034$. The σ_r evaluation allows furthermore the assesment of the non-linear growth coefficient l_r:

$$l_r = \sigma_r \times \frac{A}{|A^3|} \tag{2}$$

The sign of l_r coefficient indicates the subcritical or supercritical nature of the present instability. l_r can be evaluated near the saturation threshold. The values 3.055 and 2.314 are found for $Re = 200$ and 300 respectively, therefore the nature of the instability is subcritical (Handerson and Barkley [11]) It has been found that the rotation changes the instability nature comparing to the non-rotated case, where at $Re = 300$ the mode is supercritical, Bouhadji and Braza [5]. The evaluation of σ_r and l_r coefficients allows assessment of the real part of the Ginzburg Landau coefficient, μ_r in respect to the 3D growth. In the saturation stage, the term $\frac{\partial A}{\partial t}$ vanishes. Therefore, $\mu_r = (\sigma_r - l_r.A^2)/2$. This yields an assessment of dimensionless mu_r values: 4.43×10^{-3} and 7.26×10^{-3} for $Re = 200$ and 300 respectively. The above discussion provides the amplification characteristics of the global instability by means of the DNS approach and by simpler, global osillator model.

In the following section this paper aims at analysing the energy of the organised modes in space and time and to provide the pattern reconstruction of the coherent structures.

5. Analysis of the organised modes by the Proper Orthogonal Decomposition

The analysis of the 2D and 3D organised modes under the rotation effect has been performed by the proper orthogonal decomposition, using the snapshot method, Berkooz et al. [4]. Figures 12 compares the energy of the first 20 P.O.D. modes for the different values of α for $Re = 200$ in the 2D study A rapid energy decay is attained for both modes of instability. However, higher number of modes were needed to reproduce the flow pattern in the mode II, but a number of 20 modes are sufficient at this Reynolds number. The same study was performed for the 3D flow; figure 13 shows Compares the energy of the first 20 modes of the 2D and the 3D cases. It can be seen that the 3D energy decay is less abrupt than the 2D case. This displays a more chaotic character that is captured by the 3D DNS. While 7 modes seems to be sufficient de reconstruct the 2D flow field in the mode I, higher number of modes, of order of 20, is needed in the 3D case as shown in figure 14.

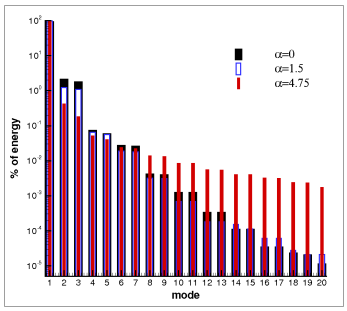

Figure 12. energy of the first 20 POD modes for different rotation rates, $Re = 200$

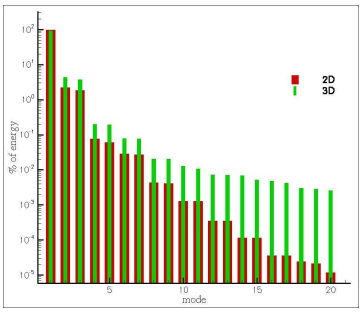

Figure 13. slope comparison of the energy contribution of the first POD modes in 2D and 3D simulations, $Re = 200$, $\alpha = 0$

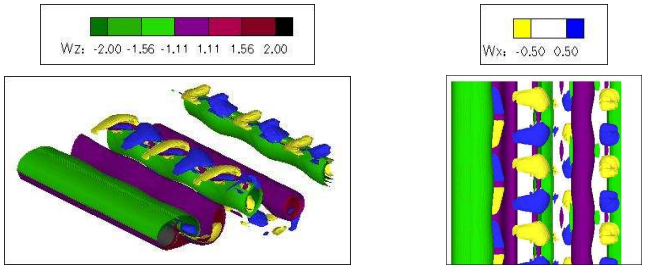

a)instantaneous field

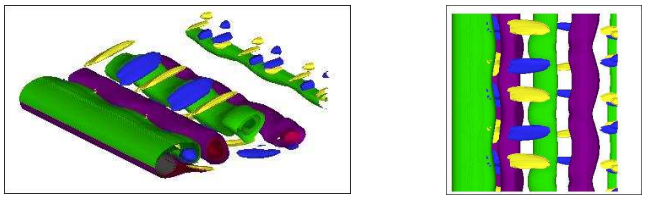

b) reconstruction with the first 3 modes

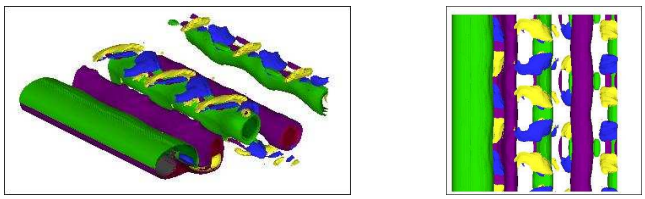

e) 19 modes

Figure 14. reconstructions of the instantaneous field with the first eigenmodes, $Re = 300$, $\alpha = 0.5$

6. Conclusion

The present study analyses the successive transition steps in the flow around rotating circular cylinder for Reynolds numbers from 40 to 500, as the rotation rate α increases from 0 to 6, by means of direct numerical simulations. For low Reynolds numbers (less than 48), the flow remains steady Increasing α causes a loss of symmetry, an increasing of the lift coefficient, and a decreasing of the drag coefficient due to the Magnus effect. Detailed flow computations have been carried out for higher Reynolds numbers (up to 500). Similar flow regimes appear as a function of Re as α increases. The Von-Kármán vortex shedding, asymmetric due to the rotation, disappears at a critical value of rotation rate, but a second mode of instability appears for a higher range of α where only counter clockwise vortices are detached. For higher rotation rates, the flow is steady again because the rotation effects keep the vortex structure near the wall and inhibit detachment. Three-dimensional computations have been carried out in order to analyse the onset of the 3D transition phenomena under the rotation effect, concerning the coherent structures in the wake. It is shown that the rotation attenuates the secondary instability and increases the critical Reynolds number of appearance of this instability. The amplification characteristics of the global instability are analysed by means of the DNS approach and by simpler, global osillator model. The analysis of the energy of the organised modes is carried out by proper orthogonal decomposition. For the 2D case, mode I reconstructions are satisfactory with an order of 9 modes, concerning the mode II, more modes were needed; an order of the 20 modes is sufficient. In the 3D case, about 15 modes are needed to capture the secondary instability. This work has a significant implications for the flow control strategies using rotating cylinders. Steady flows may occur for some intervals of rotation rates.

Acknowledgements

This work has been carried out in the research group EMT2 (Ecoulements Monophasiques, Transitionnels et Turbulents) of the Institut de Mécanique des Fluides de Toulouse. We are grateful to D. Faghani and A. Barthet concerning their collaboration in the P.O.D. approach. Part of this work is carried out on the basis of CPU allocations of the national computer centres of France CINES, CALMIP and IDRIS.

References

[1] M. A. Amsden and F. H. Harlow. The SMAC method : a numerical technique for calculating incompressible fluid flows. Los Alamos Scientific Laboratory Report. L.A. 4370, 1970.

[2] H. M. Badr, M. Coutanceau, S. C. R. Dennis, and C. Ménard. Unsteady flow past a rotating circular cylinder at reynolds numbers 10^3 and 10^4. *J. Fluid Mech.*, 220:459–484, 1990.

[3] H. M. Badr and S. C. R. Dennis. Time dependent viscous flow past an impulsively started rotating and translating circular cylinder. *J. Fluid Mech.*, 158:447–488, 1985.

[4] G. Berkooz, P. Holmes, and J. Lumley. The proper orthogonal decomposition in the analysis of turbulent flows. *Ann. Rev. Fluid Mech.*, 25:539–575, 1993.

[5] A. Bouhadji and M. Braza. Compressibility effect on the 2d and 3d vortex structures in a transonic flow around a wing. *ERCOFTAC Bull.*, 34:4–9, 1997.

[6] M. Braza, P. Chassaing, and H. Ha-Minh. Numerical study and physical analysis of the pressure and velocity fields in the near wake of a circular cylinder. *J. Fluid Mech.*, 165:79–130, 1986.

[7] C. C. Chang and R. L. Chern. Vortex shedding from an impulsively started rotating and translating circular cylinder. *J. Fluid Mech.*, 233:265–298, 1991.

[8] K. A. Cliffe and S. J. Tavener. The effect of cylinder rotation and blockage ratio on the onset of the periodic flows. *J. Fluid Mech.*, 501:125–133, 2004.

[9] M. Coutanceau and C. Ménard. Influence of the rotation on the near wake development behind an impulsively started circular cylinder. *J. Fluid Mech.*, 158:399–446, 1985.

[10] F.H. Harlow and J.E. Welch. Numerical calculation of the time-dependent viscous incompressible flow of fluids with free surface. *Phys. Fluids*, 8:2182–2189, 1965.

[11] R.D. Henderson and D. Barkley. Secondary instability in the wake of a circular cylinder. *Phys. Fluids*, 8:1683–1685, 1996.

[12] C. Mathis, M. Provansal, and L. Boyer. Bénard-von kàrmàn instability: transient and forced regimes. *J. Fluid Mech.*, 182:1–22, 1987.

[13] S. Mittal and B. Kumar. Flow past a rotating cylindre. *J. Fluid Mech.*, 476:303–334, 2003.

[14] M. T. Nair, T. K. Sengupta, and U. S. Chauchan. Flow past rotating cylinders at high reynolds numbers using higher order upwiwnd scheme. *Comput. Fluids*, 27:47–70, 1998.

[15] D.W. Peaceman and J.R. Rachford. The numerical solution of parabolic and elliptic differential equations. *J. Soc. Indust. Appli. Math.*, 3:28, 1955.

[16] H. Persillon and M. Braza. Physical analysis of the transition to turbulence in the wake of a circular cylinder by three-dimensional navier-stokes simulation. *J. Fluid Mech.*, 365:23–88, 1998.

[17] L. Prandtl. Application of the "magnus effect" to the wind propulsion of ships. *Die Naturwissenschaft*, 13:93–108, 1925. Trans. NACA-TM-367, june 1926.

[18] E. G. Reid. Tests of rotating cylinders. Technical Report NACA-TN-209, 1924.

[19] D. Stojković, M. Breuer, and F. Durst. Effect of high rotation rates on the laminar flow around a circular cylinder. *Phys. Fluids*, 14:3160–3178, 2002.

[20] D. Stojković, P.Schön, M. Breuer, and F. Durst. On the new vortex shedding mode past a rotating circular cylinder. *Phys. Fluids*, 8:1683–1685, 2003.

[21] A. Thom. The pressure round a cylinder rotating in an air current. (ARC R. & M. 1082), 1926.

[22] A. Thom. Experiments on the flow past a rotating cylinder. (ARC R. & M. 1410), 1931.